Atmos. Chem. Phys. Discuss., 13, 28729–28749, 2013
www.atmos-chem-phys-discuss.net/13/28729/2013/
doi:10.5194/acpd-13-28729-2013

Atmospheric Chemistry and Physics Discussions
Open Access

Perturbations in relative humidity in the boundary layer represent a possible mechanism for the formation of small convective clouds

E. Hirsch[1,2], I. Koren[1], O. Altaratz[1], Z. Levin[3,4], and E. Agassi[2]

[1]Department of Earth and Planetary Sciences, Weizmann Institute, Rehovot 76100, Israel
[2]Department of Environmental Physics, Israel Institute for Biological Research, Nes-Ziona, Israel
[3]Department of Geophysical, Atmospheric and Planetary Sciences, Tel-Aviv University, Tel-Aviv, Israel
[4]The Energy, Environment and Water Research Center (EEWRC), The Cyprus Institute, Nicosia, Cyprus

Received: 17 October 2013 – Accepted: 24 October 2013 – Published: 4 November 2013

Correspondence to: I. Koren (ilan.koren@weizmann.ac.il)

Published by Copernicus Publications on behalf of the European Geosciences Union.

Abstract

An air parcel model was developed to study the formation of small convective clouds that appear under conditions of weak updraft and a strong thermal inversion layer above the clouds. Observations suggest that these clouds are characterized by a cloud base height far lower than the lifting condensation level. Considering such atmospheric conditions, the air parcel model shows that these clouds cannot be the result of classical thermals or plumes that are caused by perturbations in the temperature near the surface. We suggest that such clouds are the result of perturbations in the relative humidity of elevated air pockets. These results explain the existence of small clouds that standard methods fail to predict and shed light on processes related to the formation of convective clouds from the lowest end of the size distribution.

1 Introduction

Convective clouds form when an air parcel rises in an atmospheric column, cools and reaches supersaturation. Typically, air parcels are assumed to take the form of thermals or plumes that start the convective motion near the surface (Pruppacher and Klett, 1998; Turner, 1969). Conventionally, two atmospheric thermodynamic parameters are used to predict the base height of clouds for a given atmospheric profile (under dry adiabatic assumptions): the lifting condensation level (LCL, see Bolton, 1980) dictates the pressure and the temperature of the parcel as it ascends (owing to external forcing) and reaches saturation. The convective condensation level (CCL) dictates the height of the saturation level for a parcel that is forced by surface heating. Because the relative humidity of the parcel decreases as its temperature increases, the CCL is usually higher than the LCL. By definition, the LCL and CCL are strongly correlated with the base height of the convective cloud. Many convective thermals have been shown to be characterized by undiluted cores (Stull, 1988); thus, the actual cloud base is very close to the LCL, which is calculated when air parcels are lifted from near the surface.

ACPD
13, 28729–28749, 2013

Therefore, the LCL is regularly used to predict the expected vertical position of clouds (Craven and Jewell, 2002). Although the LCL height is useful, it is unable to predict the likelihood of cloud formation because it does not take into account the actual atmospheric conditions along the vertical path of the parcel. For example, a strong inversion layer below the LCL can block the vertical motion of a rising parcel and prevent it from becoming a cloud. The atmospheric profile shown in Fig. 1 presents a typical midday summertime profile for the eastern Mediterranean region: hot and humid air capped by an inversion layer. A comparison of the inversion layer in the atmospheric profile with the position of the higher LCL does not predict cloud formation.

On many summer days in these regions, small (100 m scale) cumulus clouds are not uncommon, even though the base of the inversion layer is below the LCL. Such clouds were observed (Fig. 2) during a field campaign in the summer of 2011. During that period, the atmospheric profile and cloud base height was measured by the IMS station at Bet-Dagan which is located ~ 10 km away from the location of the field campaign. In such instances, ceilometer measurements of the cloud base height reveal a discrepancy between the measured height and the theoretical LCL height. Specifically, for the atmospheric profile shown in Fig. 1, although the LCL was 1290 m, the ceilometer readings reported that the cloud base height was 700 m – approximately 590 m below the LCL and below the atmospheric inversion layer as well. In light of this discrepancy, this study was conducted to examine how convective clouds can form far below the standard LCL height and to analyze the conditions that allow them to form.

An air parcel model is a commonly used tool for studies of basic cloud formation processes. This type of model follows the vertical motion and evolution of an air parcel by focusing on detailed descriptions of some processes and approximate descriptions of other processes that are supposedly less relevant to the specific study. For example, air parcel models can be used to study the effects of environmental conditions on the fraction of activation in clouds (Reutter et al., 2009), to examine the temporal evolution in the size distribution of droplets within a cloud (Simmel and Wurtzel, 2006; Volke

ACPD
13, 28729–28749, 2013

et al., 2005) and to study the effect of entrainment on the size distribution of droplets (Khain et al., 2000).

As described in Sect. 2, the air parcel model developed for this study uses the most fundamental thermodynamic and microphysical equations. The model follows the development of a rising parcel of moist air that starts as a pocket of humidified aerosols with a given size distribution and ends as a cloud. The model outputs and data collected during a field campaign focused on such clouds were analyzed and validated.

2 Methods

In our theoretical analysis, we developed an air parcel model based on the following equations that combine the vertical motion of a rising moist air parcel with the diffusional growth of humidified aerosols and water droplets within the parcel. All air parcel models implement some form of the first law of thermodynamics, usually as follows (Wallace and Hobbs, 2006):

$$\mathrm{d}T = \frac{1}{c_p}\left(\mathrm{d}q + RT\frac{\mathrm{d}p}{p}\right). \tag{1}$$

(See Appendix Table A1 for a complete description of the symbols.)

Equation (1) describes changes in the parcel temperature ($\mathrm{d}T$); $\mathrm{d}T$ increases with the release of latent heat that occurs as water vapor condenses ($\mathrm{d}q$) and cools as a result of the expansion of the parcel ($RT\mathrm{d}p/p$). The latent heat released by inactivated haze droplets is incorporated into the model by means of a detailed scheme that treats the growth of humidified aerosols.

The growth rate of every haze or cloud droplet is determined by a diffusion equation that depends on the difference between the ambient relative humidity (or supersaturation) in the air parcel ($S_{\mathrm{v,\,w}}$) and the relative humidity adjacent to the droplet (Köhler, 1936). The growth rate also depends on the heat conductivity and diffusion coefficients

ACPD
13, 28729–28749, 2013

of the condensing water droplets. These relationships are described by Pruppacher and Klett (1998) as follows:

$$r\frac{\mathrm{d}r}{\mathrm{d}t} = \frac{D_v^* M_w e_{sat,\,w}(T_\infty)}{\rho_s'' RT} \left(S_{v,w} - \frac{1}{1+\delta} \exp\left[\frac{L_e M_w}{RT}\left(\frac{\delta}{1+\delta}\right) + \frac{2M_w \sigma_{s/a}}{RT(1+\delta)\rho_w r} - \frac{\upsilon \Phi_s \varepsilon_m M_w \rho_N r_N^3}{M_s \rho_w \left(r^3 - r_N^3\right)} \right] \right) \tag{2}$$

The rate of depends on two competing processes. The supersaturation increases when the air parcel cools as it ascends and decreases when vapor is depleted by the condensational growth of the haze and cloud droplets (Lee and Pruppacher, 1977):

$$\frac{\mathrm{d}s_{v,\,w}}{\mathrm{d}t} = \frac{p}{\varepsilon e_{sat,\,w}} \frac{\mathrm{d}w_v}{\mathrm{d}t} - (1 + s_{v,\,w}) \left(\frac{\varepsilon L_e}{R_a T^2} \frac{\mathrm{d}T}{\mathrm{d}t} + \frac{g}{R_a T} U \right) \tag{3}$$

The rate of change in the updraft of the parcel (U) is derived from momentum considerations (Lee and Pruppacher, 1977). A positive thermal contrast between the parcel and the environment accelerates the parcel, while the drag force resulting from the condensing water decelerates the parcel. The following term represents the effect of the entrained air on the updraft:

$$\frac{\mathrm{d}U}{\mathrm{d}t} = \frac{g}{1+\gamma} \left(\frac{T_v - T_v'}{T_v'} - W_L \right) - \mu_J U^2 \tag{4}$$

The inputs to the model are the atmospheric profiles (temperature, relative humidity and pressure), the initial conditions of the parcel (vertical position, initial relative humidity, initial temperature and initial updraft) and the size distribution and chemical composition of the dry aerosol. The model calculates the temporal evolution of the vertical position, temperature, relative humidity, updraft and the size distribution of the

ACPD
13, 28729–28749, 2013

growing water droplets of the parcel. The cloud base height was determined from the model results for a relative humidity level of 100 %.

In our model, the input data for the dry aerosol size distribution are based on number size distributions measured in Europe (Asmi et al., 2011). The distribution is represented by a discrete 250-bin parameterization sampled on a logarithmic scale. Because the influence of the size distribution of the aerosols on the cloud's properties greatly exceeds that of the chemistry of the aerosols (Reutter et al., 2009; Dusek et al., 2006), we assumed that all of the aerosols are ammonium sulfate; this assumption also allowed us to simplify the model. Furthermore, because the deliquescence relative humidity of ammonium sulfate is approximately 80 % (Brooks et al., 2002), we can assume that aerosols take up water vapor by diffusion in the very early stages of air parcel movement. To increase the accuracy of the model, we used a fine temporal resolution of 2.5 ms.

In addition to building the air parcel model, we used measurements obtained by the Israeli Meteorological Service (IMS). The IMS station at Bet-Dagan is located 10 km east of the Mediterranean shore and measures the atmospheric profile on a daily basis by releasing a radiosonde at 12:00 UTC (15:00 LT during the summer). These sounding atmospheric profiles (website: atmospheric sounding) served two purposes: first, they were used as inputs for the air parcel model; and second, they were used to calculate the LCL. The LCL itself was derived by two different methods: (1) the method used by the University of Wyoming (website: sounding station parameters and indices), which uses the average value of the lower 500 m of the atmosphere (referred to hereafter as the average LCL); and (2) the standard formalism described by Bolton (1980) and Stull

ACPD
13, 28729–28749, 2013

(1988):

$$T_{\mathrm{LCL}} = \frac{1}{\frac{1}{T_k - 55} - \frac{\ln\left(\frac{\mathrm{RH}}{100}\right)}{2840}} + 55 \tag{5}$$

$$P_{\mathrm{LCL}} = P\left(\frac{T_{\mathrm{LCL}}}{T_k}\right)^{3.5}$$

where T_k, P and RH are the temperature, pressure and relative humidity, respectively, of the air parcel at the ground level (referred to hereafter as the ground LCL).

The IMS also continuously measures cloud base heights with a commercial ceilometer (Vaisala Model CL31). A 2 h average of the 10 min readings was used as a reference to determine the cloud base height during the time for which the atmospheric profiles were measured.

3 Results

Conventionally, it is assumed that mechanical forcing or perturbations in temperature cause air parcels to rise in the atmosphere (Pruppacher and Klett, 1998; Turner, 1969). We ran the air parcel model with two schemes representing different initial conditions. In the first scheme, the air parcel was subjected to a perturbation in initial temperature (compared to the ambient conditions), as is usually the case in air parcel models. As previously described, such perturbations correspond to CCL calculations.

Increases in parcel temperatures are not the only mechanism by which positive buoyancy can be generated. Increases in the relative humidity of the parcel decrease the density of the parcel, resulting in an increase in the buoyancy of the parcel. Therefore, in the second initialization scheme, the parcel was subjected to a perturbation in relative humidity (relative to that of ambient conditions). Because the studied region is characterized by a flat terrain a few kilometers away from the shore, no initial updraft was provided to the parcels in either scheme.

Figure 3 presents the results of the air parcel model for 6 August 2011. The sounded atmospheric profile (the blue and red lines represent temperature and RH profiles, respectively) was used as an input for the model and the parcel was initiated at various heights (50 m to 700 m in increments of 50 m). The results of the initialization scheme involving temperature perturbations are presented in Fig. 3a, b, while the results of the initialization scheme involving RH perturbations are presented in Fig. 3c, d. In Fig. 3a, the plotted results span the predicted elevation of the cloud base (determined for 100 % relative humidity) for a set of temperature perturbations of parcels along the vertical column. At every initial height, the parcel was subjected to a variety of perturbations in temperature relative to the environmental temperature (0.25 °C to 10 °C in increments of 0.25 °C). For every simulated case with a specific initial height and thermal perturbation, we assessed whether the air parcel had reached saturation. The colored region in Fig. 3a corresponds to the cloud base height predicted by the air parcel model for different initial heights and perturbations in the temperature of the parcel. The black region represents perturbations that were insufficient to produce clouds (i.e., the parcel did not reach saturation level). The figure reveals a range of possible cloud base heights of 1300 m to 2500 m. In this type of initialization (characterized by perturbations in the temperature of the parcel), it is not possible for clouds to form below 1300 m. Therefore, such a mechanism cannot explain the existence of clouds at the actual measured height (697 m). Figure 3b presents more details of the simulated results of the air parcel model for the schemes of temperature perturbation. The paired colored symbols in Fig. 3b represent the results for each initial height. The lower symbol of every pair represents the initial height of the parcel and the size of the smallest perturbation that caused a parcel to become a cloud. The higher mark of every pair represents the height of the parcel when saturation was reached (i.e., the cloud base height). For example, the pair of blue circles represents an air parcel that started ascending at 50 m and was subjected to a perturbation of 1.25 °C. The cloud base height in this case was 1338 m (the upper blue circle). Similarly, a parcel that started at 100 m with a perturbation of 2.75 °C (red circles) reached saturation and created a cloud. The cloud base heights

ACPD
13, 28729–28749, 2013

Perturbations in relative humidity in the boundary layer

E. Hirsch et al.

are higher than the two types of calculated LCL and much higher than the measured cloud base. As previously explained, temperature perturbations correspond to the CCL, and the CCL is expected to be higher than the LCL. Our model predicts that perturbations in the temperature of the parcel cannot lead to the formation of clouds at the actual measured height regardless of the initial height of the parcel and magnitude of the thermal perturbation.

The results predicted by the model for perturbations in the relative humidity of the parcel (Fig. 3c, d) were completely different. At every initial height, the parcel was subjected to a variety of perturbations in relative humidity (from the ambient RH to 99 % in increments of 1 %). For every simulated case with a specific initial height and RH perturbation, we assessed whether the air parcel had reached saturation. Figure 3c reveals a range of possible cloud base heights between 100 m and 1100 m. Figure 3d presents a more detailed view of the results generated by perturbations in relative humidity; the smallest perturbations in the RH that lead to cloud formation are presented. The results shows that air parcels that started at the surface layer (in the lower 150 m) cannot form clouds at the measured height (697 m). However, all of the parcels that began to ascend at 200–600 m and were subjected to a perturbation in relative humidity of 5.5–8.2 % could create clouds at the actual measured height. Such perturbations in relative humidity are realistic. Previous studies have shown that the temporal behavior of humidity is dominated by atmospheric turbulence and follows the predicted −5/3 power law (e.g., Filho et al., 1988). In addition, coastal measurements of the absolute humidity near the surface in Denmark documented rapid fluctuations of 5.8–7.4 $g\,m^{-3}$, which correspond to a relative humidity of 34–43 % for an air temperature of 20 °C (Sempreviva and Gryning, 1996).

Similar results were obtained for the atmospheric profile for 11 June 2011 at 12:00 UTC. While the LCL calculations predicted the cloud base to be at 1278 m and 1161 m for the ground and average LCL, respectively, the ceilometer reading indicated a cloud base height of 884 m. As was observed previously, perturbations in the temperature of the parcel failed to explain the existence of clouds at the measured height

ACPD
13, 28729–28749, 2013

(Fig. 4), while perturbations in the relative humidity of parcels that ascended from the middle of the boundary layer resulted in cloud formation at heights similar to the measured height (Fig. 5).

How common are these clouds? Figure 6 presents the LCL (red) and measured cloud base height (blue) during the summer months in the studied region. On 27 of 92 days, the presence of clouds was documented from 11:00 UTC to 13:00 UTC. The measured cloud base height was lower than the LCL on all 27 of these days, with an average difference of 363 m. This finding suggests that the conditions considered in the case studies are not atypical and that the existence of clouds below their LCL is quite common. Furthermore, the air parcel model was used to calculate the expected cloud base height for every atmospheric profile. Using the RH perturbations scheme and initiating all the air parcels from 400 m, provides cloud base heights (green circles in Fig. 6) which are very similar to the measured cloud base height (blue circles in Fig. 6). The initial height of 400 m was chosen since in the detailed case study (which was presented in Fig. 3) the range of 200–600 m provided accurate results in terms of expected cloud base heights. The average absolute difference between the calculated and measured cloud base height is ~ 70 m. This finding suggests that the proposed mechanism of RH perturbations provides possible explanation to the existence and vertical extent of small clouds under wide range of atmospheric conditions.

4 Discussion and summary

In this paper, we presented detailed case studies of small convective cloud formation in instances in which the boundary layer inversion base was below the predicted LCL (thus theoretically blocking any cloud formation) and when the measured cloud bases were far below the expected LCL. Using a detailed air parcel model, we showed that the presence of such clouds cannot be explained by air parcels that are driven from the ground by thermal perturbations. More importantly, the model shows that these clouds are most likely the result of ascending air parcels that were forced upwards

ACPD
13, 28729–28749, 2013

by perturbations in the relative humidity. We also show that such conditions and such clouds are common during the summer in the eastern Mediterranean region.

A hot and humid boundary layer that is capped by a strong inversion layer is not unique to the summertime in the eastern Mediterranean region. Many coastal places along the subtropical belts can be characterized by such conditions at some time during the year. Two examples for such conditions are shown in Fig. 7. The sounding atmospheric profile, the measured cloud base height and the average and ground LCL are presented for Palma de Mallorca (39.61° N, 2.71° E) on 11 August 2011 at 12:00 UTC (left) and for Tenerife (28.47° N, 16.38° W) on 23 August 2011 at 12:00 UTC (right).

These findings provide insights into processes that occur in the boundary layer. It is commonly assumed that convective clouds are the result of plumes or thermals originating near the surface layer arising from mechanical forcing or perturbations in the temperature. The results of this study suggest that for some atmospheric conditions, cloud formation can be initiated by the elevation of air parcels that have been subjected to perturbations in RH along the vertical column within the boundary layer.

For a given set of environmental conditions, the maximum size and life span of clouds should be scaled to the magnitude of the perturbation that created them. The delicate RH perturbations that can occur not far below the cloud base add another level of freedom to boundary layer cloud formation. This information can be used to predict the formation of very small-sized clouds (of the order of tens of meters) that exist for very short durations (on a scale of minutes). Most space-borne sensors that are used for purposes of atmospheric research lack the required resolution to detect such clouds. Therefore, it is likely that sparse coverage of small clouds will be designated a cloud-free field and the contribution of these clouds will be attributed falsely to the cloud-free atmosphere (Koren et al., 2007). The cloud formation described here confirms that a robust way to measure and study very small clouds is necessary.

Acknowledgements. The research leading to these results was conducted with funding from the European Research Council under the European Union's Seventh Framework Programme (FP7/2007-2013)/ERC Grant agreement n° [306965].

ACPD
13, 28729–28749, 2013

We thank the Department of Atmospheric Sciences of the University of Wyoming for the sounding data (downloaded from http://weather.uwyo.edu/upperair/sounding.html) and the Israeli Meteorological Service (IMS) for providing the ceilometer cloud base height readings.

References

Asmi, A., Wiedensohler, A., Laj, P., Fjaeraa, A.-M., Sellegri, K., Birmili, W., Weingartner, E., Baltensperger, U., Zdimal, V., Zikova, N., Putaud, J.-P., Marinoni, A., Tunved, P., Hansson, H.-C., Fiebig, M., Kivekäs, N., Lihavainen, H., Asmi, E., Ulevicius, V., Aalto, P. P., Swietlicki, E., Kristensson, A., Mihalopoulos, N., Kalivitis, N., Kalapov, I., Kiss, G., de Leeuw, G., Henzing, B., Harrison, R. M., Beddows, D., O'Dowd, C., Jennings, S. G., Flentje, H., Weinhold, K., Meinhardt, F., Ries, L., and Kulmala, M.: Number size distributions and seasonality of submicron particles in Europe 2008–2009, Atmos. Chem. Phys., 11, 5505–5538, doi:10.5194/acp-11-5505-2011, 2011.

Atmospheric sounding: available at: http://weather.uwyo.edu/upperair/sounding.html, (last access: 1 October 2013), 2013.

Bolton, D.: The computation of equivalent potential temperature, Mon. Weather Rev., 108, 1046–1053, doi:10.1175/1520-0493(1980)108<1046:tcoept>2.0.co;2, 1980.

Brooks, S. D., Wise, M. E., Cushing, M., and Tolbert, M. A.: Deliquescence behavior of organic/ammonium sulfate aerosol, Geophys. Res. Lett., 29, 1917, doi:10.1029/2002GL014733, 2002.

Craven, J. P., Jewell, R. E., and Brooks, H. E.: Comparison between observed convective cloud-base heights and lifting condensation level for two different lifted parcels, Weather Forecast., 17, 885–890, 2002.

Dusek, U., Frank, G., Hildebrandt, L., Curtius, J., Schneider, J., Walter, S., Chand, D., Drewnick, F., Hings, S., and Jung, D.: Size matters more than chemistry for cloud-nucleating ability of aerosol particles, Science, 312, 1375–1378, 2006.

Khain, A., Ovtchinnikov, M., Pinsky, M., Pokrovsky, A., and Krugliak, H.: Notes on the state-of-the-art numerical modeling of cloud microphysics, Atmos. Res., 55, 159–224, 2000.

Köhler, H.: The nucleus in and the growth of hygroscopic droplets, T. Faraday Soc., 32, 1152–1161, 1936.

Koren, I., Remer, L. A., Kaufman, Y. J., Rudich, Y., and Martins, J. V.: On the twilight zone between clouds and aerosols, Geophys. Res. Lett., 34, 2007.
Lee, I.-Y. and Pruppacher, H.: A comparative study on the growth of cloud drops by condensation using an air parcel model with and without entrainment, Pure Appl. Geophys., 115, 523–545, 1977.
Medeiros Filho, F., Jayasuriya, D., Cole, R., Helmis, C., and Asimakopoulos, D.: Correlated humidity and temperature measurements in the urban atmospheric boundary layer, Meteorol. Atmos. Phys., 39, 197–202, 1988.
Pruppacher, H. R., Klett, J. D., and Wang, P. K.: Microphysics of Clouds and Precipitation, Springer, New York, 1998.
Reutter, P., Su, H., Trentmann, J., Simmel, M., Rose, D., Gunthe, S. S., Wernli, H., Andreae, M. O., and Pöschl, U.: Aerosol- and updraft-limited regimes of cloud droplet formation: influence of particle number, size and hygroscopicity on the activation of cloud condensation nuclei (CCN), Atmos. Chem. Phys., 9, 7067–7080, doi:10.5194/acp-9-7067-2009, 2009.
Roland, B. S.: An Introduction to Boundary Layer Meteorology, Kluwel'Academic Publishers, Boston, 1988.
Sempreviva, A. M. and Gryning, S.-E.: Humidity fluctuations in the marine boundary layer measured at a coastal site with an infrared humidity sensor, Bound.-Lay. Meteorol., 77, 331–352, 1996.
Simmel, M. and Wurzler, S.: Condensation and activation in sectional cloud microphysical models, Atmos. Res., 80, 218–236, 2006.
Sounding station parameters and indices: available at: http://weather.uwyo.edu/upperair/indices.html (last access: 1 October 2013), 2013.
Turner, J. S.: Buoyant plumes and thermals, Annu. Rev. Fluid Mech., 1, 29–44, doi:10.1146/annurev.fl.01.010169.000333, 1969.
Wallace, J. M. and Hobbs, P. V.: Atmospheric Science: An Introductory Survey, Academic Press, London, UK, 2006.
Wolke, R., Sehili, A., Simmel, M., Knoth, O., Tilgner, A., and Herrmann, H.: SPACCIM: a parcel model with detailed microphysics and complex multiphase chemistry, Atmos. Environ., 39, 4375–4388, 2005.

ACPD
13, 28729–28749, 2013

Table A1. List of symbols

Symbol	Quantity
T	Air temperature inside the parcel
q	Latent heat release
R	Gas constant for 1 mole of ideal gas
p	Pressure
r	Droplet radius
D_v^*	Modified diffusivity of water vapor in air
M_w	Molecular weight of water
$e_{sat,w}$	Saturation vapor pressure over a plane water surface
ρ_s''	Density of aqueous salt solution
$S_{v,w}$	Supersaturation of moist air with respect to a plane water surface
L_e	Latent heat of evaporation of pure water
$\sigma_{s/a}$	Surface tension of an aqueous solution drop against air
ρ_w	Density of water
υ	Number of ions into which a salt molecule dissociates in water
Φ_s	Osmotic coefficient
ρ_N	Density of dry aerosol
r_N	Radius of dry aerosol
ε	Molecular weight ratio of H_2O to dry air (= 0.622)
w_v	Mixing ratio of unsaturated moist air
L_e	Latent heat of evaporation of pure water
R_a	Gas constant for 1 g of dry air
g	Acceleration of gravity
U	Vertical velocity of air parcel
γ	= 0.5 correction for induced mass acceleration (Pruppacher and Klett, 1998)
T_v	Virtual temperature of air parcel
T_v'	Virtual temperature of environment
W_L	Liquid water content in air parcel
μ_J	Entrainment rate for a convective plume

ACPD
13, 28729–28749, 2013

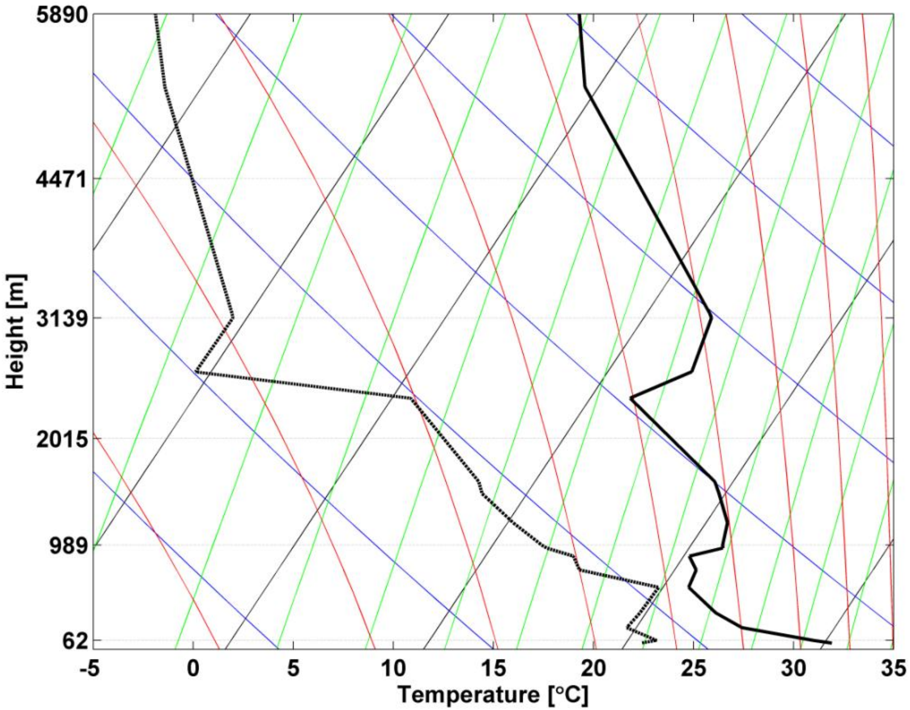

Fig. 1. Skew-T plot of the sounding atmospheric profile measured by the IMS (Israeli Meteorological Service) at the Bet-Dagan station on 6 August 2011 at 12:00 UTC (15:00 LT). The LCL is calculated to be at 870 hPa (which corresponds to 1287 m), whereas the low inversion layer is located at approximately 900 m. Such conditions suggest no cloud formation.

ACPD
13, 28729–28749, 2013

Fig. 2. Infrared image of small cumulus clouds acquired on 6 August 2011 at 14:53 LT. The color bar values indicate radiative temperatures (in °C). The radiative temperature of the left cloud is 23 °C. The camera was pointed toward the zenith and the horizontal field of view of the image (in the plane of the cloud) is 100 m. The image was acquired during a field campaign in which the atmospheric profile and cloud base height was measured approximately 10 km away at the IMS station at Bet-Dagan.

ACPD
13, 28729–28749, 2013

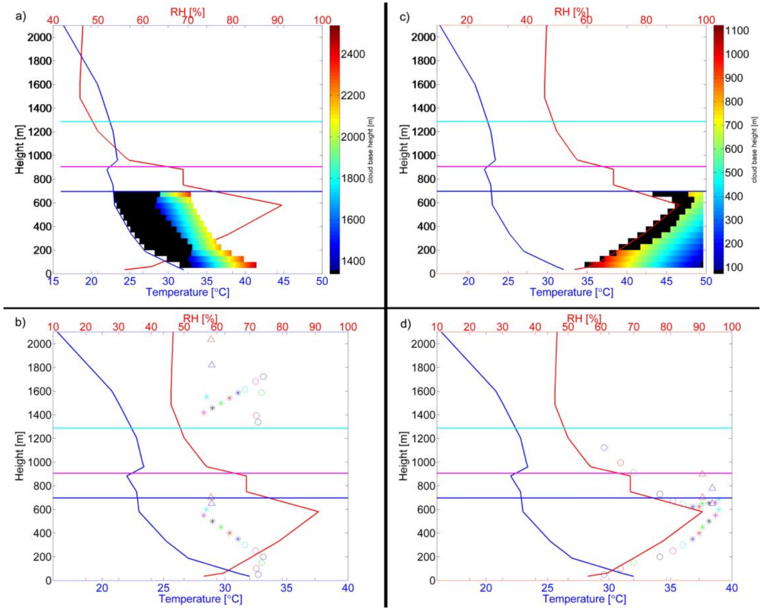

Fig. 3. Model results for the atmospheric profile of 6 August 2011. The blue and red lines represent the temperature and RH sounding profiles, respectively, on 6 August 2011 at 12:00 UTC. The horizontal cyan and magenta lines represent the ground and average LCL, respectively, and the blue line represents the measured cloud base height. Note the inversion layer at 900 m. (**a** and **b**) present the results for perturbations in the temperature of the parcel and (**c** and **d**) present the results for perturbations in the RH of the parcel. The colored regions in (**a** and **c**) represent the predicted cloud base height for various initial heights and perturbations. The initial parcel height and the magnitude of the perturbation are represented by the location on the graph. The black region indicates perturbations that do not result in cloud formation. The paired symbols in (**b** and **d**) represent the air parcel model results for various initial heights and perturbations and the cloud base heights of the resulting clouds (as explained in the text).

ACPD
13, 28729–28749, 2013

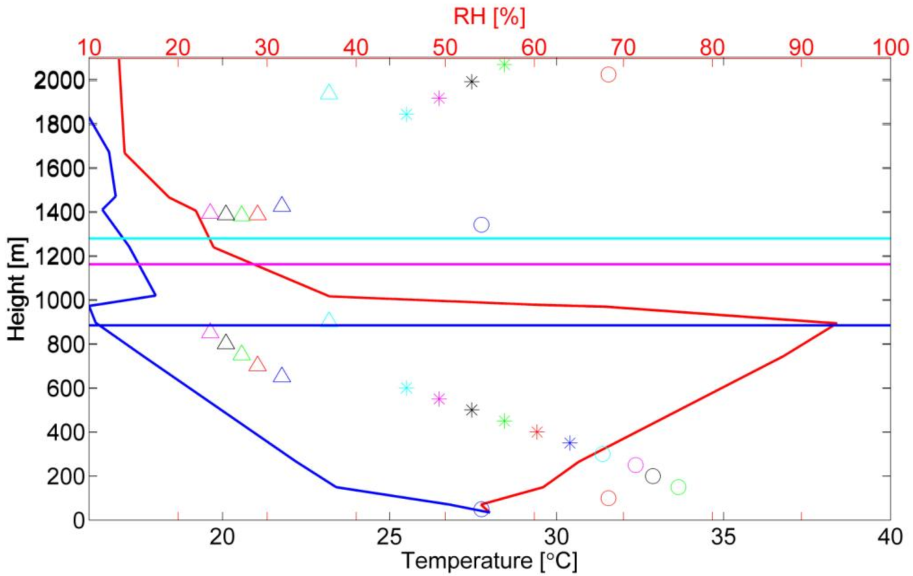

Fig. 4. Model results for perturbations in the temperature of the parcel. The blue and red lines represent the temperature and RH sounding profiles, respectively, for 11 June 2011 at 12:00 UTC. The horizontal cyan and magenta lines represent the ground and average LCL, respectively, and the blue line represents the cloud base height. The paired symbols represent the air parcel model results for various initial heights and perturbations and the cloud base heights of the resulting clouds (as explained in the text).

ACPD
13, 28729–28749, 2013

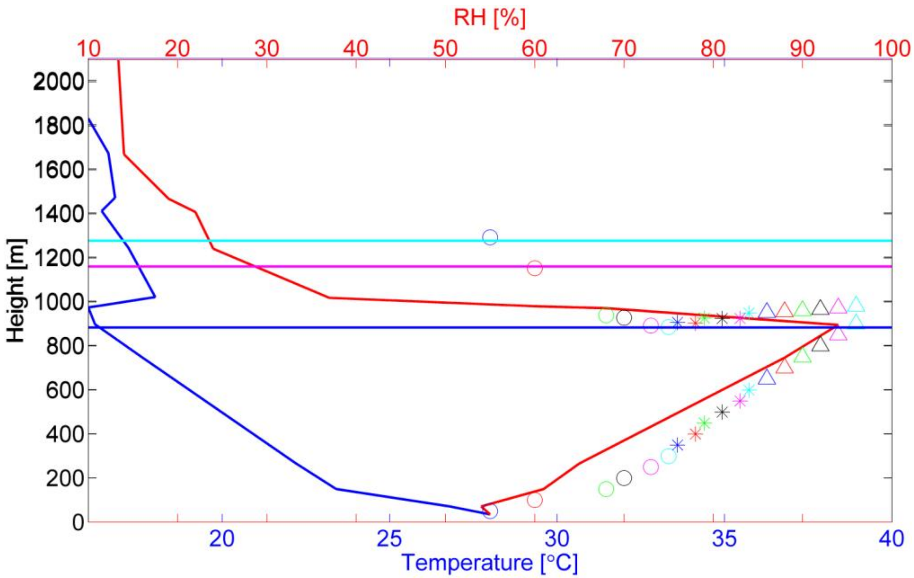

Fig. 5. This figure represents the same parameters depicted in Fig. 4 for initial perturbations in the relative humidity of the parcel.

ACPD
13, 28729–28749, 2013

Perturbations in relative humidity in the boundary layer

E. Hirsch et al.

Title Page
Abstract
Introduction
Conclusions
References
Tables
Figures
◀
▶
Back
Close
Full Screen / Esc
Printer-friendly Version
Interactive Discussion

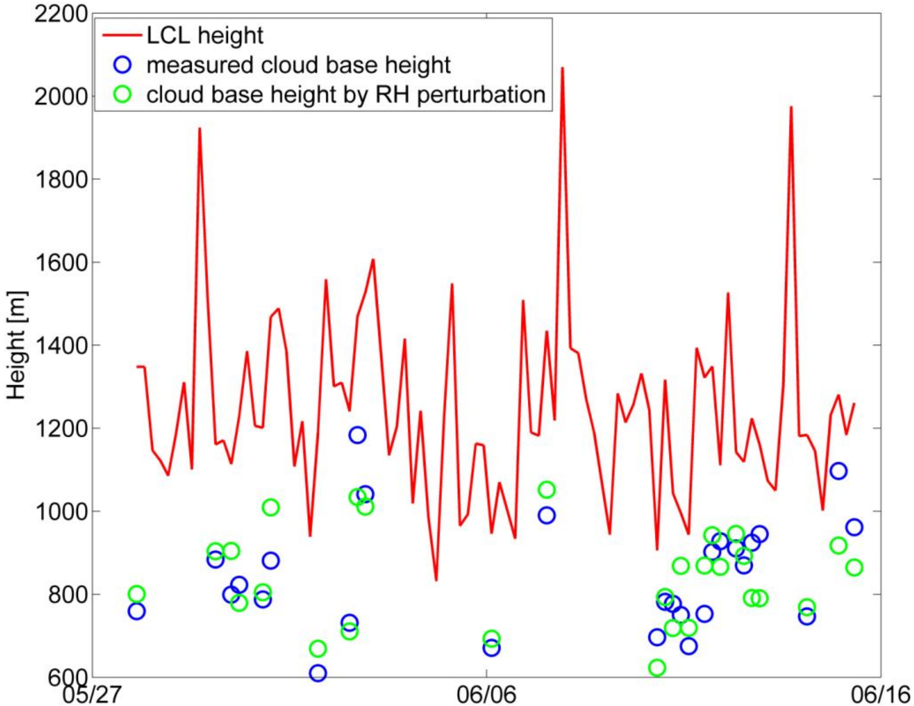

Fig. 6. Comparison of the LCL height (red) and measured cloud base height (blue) between June and August 2011. In addition, the green circles represent the cloud base height that was calculated by the air parcel model under the RH perturbations scheme. The LCL height was calculated for the Bet-Dagan sounding atmospheric profile, which was measured on a daily basis at 12:00 UTC (15:00 LT). The cloud base height is the average value of the ceilometer measurements taken between 11:00 UTC and 13:00 UTC.

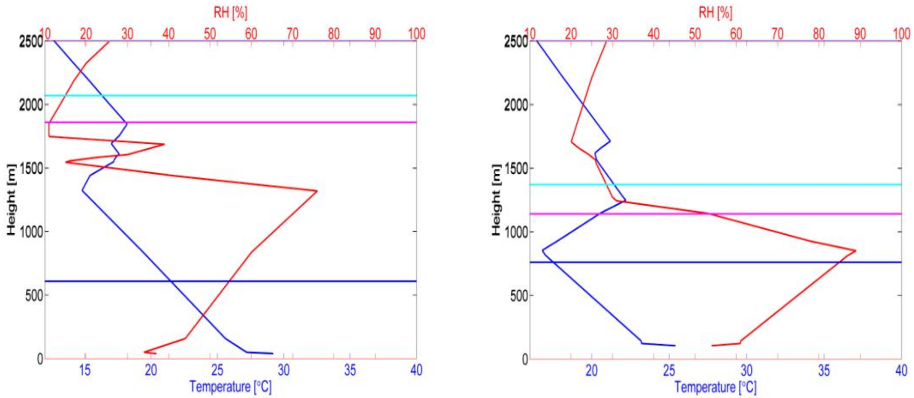

Fig. 7. Atmospheric profiles, LCL and cloud base height at Palma de Mallorca on 11 August 2011 at 12:00 UTC (left) and at Tenerife on 23 August 2011 at 12:00 UTC (right). The plot legends are identical to those described in Fig. 3. Note the inversion layer that creates a layer of high relative humidity and the discrepancy between the LCL and the measured cloud base height.

ACPD
13, 28729–28749, 2013

Perturbations in relative humidity in the boundary layer

E. Hirsch et al.